Supporting Information

Molecularly Modulated π-Conjugated Carbon Nitride Heterojunction for Efficient Photocatalytic C-C Bond Cleavage in Lignin Model

Gelan Wang,‡[a] Peihe Li,‡*[a] Chen Chen,[a] Na Liu,[a] Ye Lu,[a] Shuai Zhu,[a] Limei Duan,[a] Yuliang Li,[c] Sarina Sarina,[b] and Jinghai Liu*[a]

[a]Inner Mongolia Key Laboratory of Solid State Chemistry for Battery, Inner Mongolia Engineering Research Center of Lithium-Sulfur Battery Energy Storage, College of Chemistry and Materials Science, Inner Mongolia Minzu University, Tongliao, 028000, China.

[b]School of Chemical and Biomolecular Engineering, Faculty of Engineering, The University of Sydney, Camperdown, NSW 2037, Australia.

[c]Key Laboratory of Subsurface Hydrology and Ecological Effects in Arid Region, Ministry of Education, School of Water and Environment, Chang'an University Xi'an, 710064, China.

Table of Contents

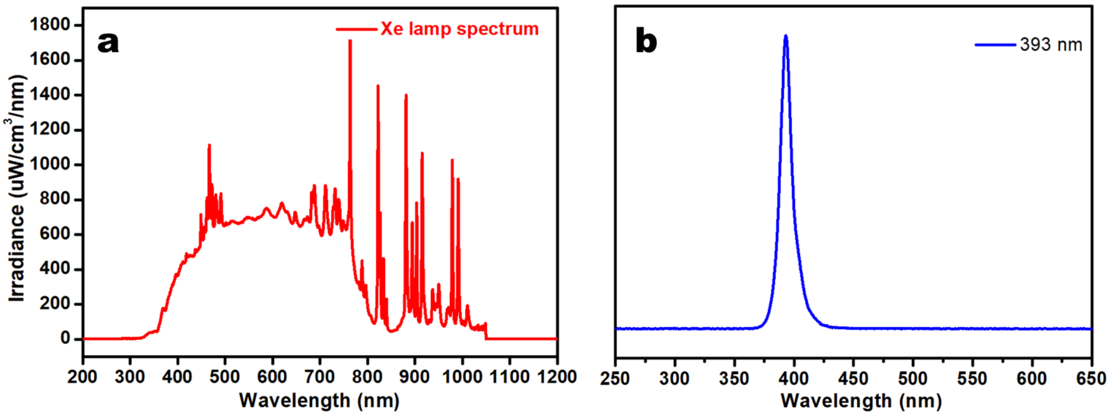

Figure S1. The sources of light. (a) Xe lamp spectrum, (b) 393 nm LEDs spectrum

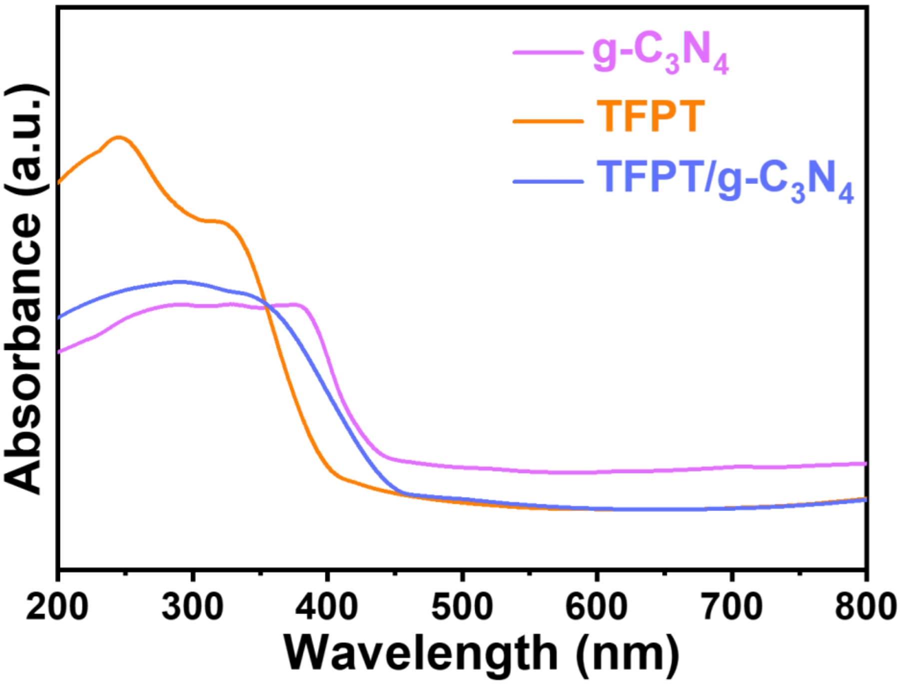

Figure S2. UV-Vis spectra of TFPT, g-C_3N_4 and TFPT/g-C_3N_4.

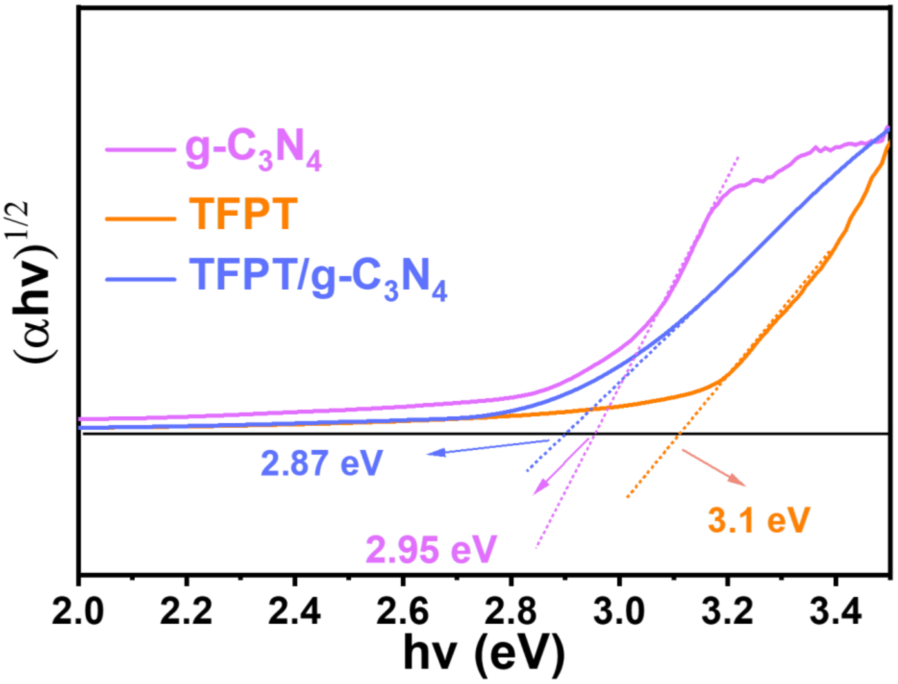

Figure S3. Bandgap of the TFPT, g-C_3N_4 and TFPT/g-C_3N_4 obtained from the UV/Vis DR spectrum according to the Kubelka–Munk theory.

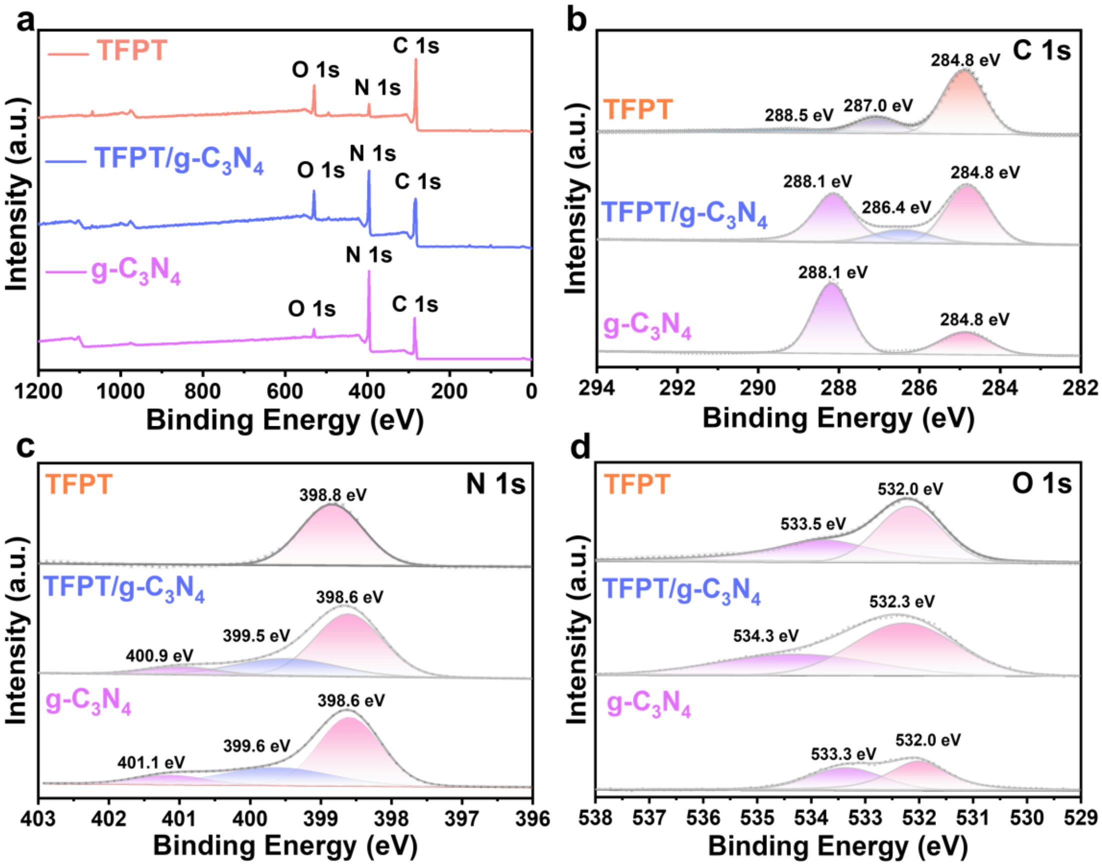

Figure S4. XPS spectra: (a) A whole scanning XPS spectra. (b) C 1s of the TFPT, g-C_3N_4 and TFPT/g-C_3N_4. (c) N 1s of the TFPT, g-C_3N_4 and TFPT/g-C_3N_4. (d) O 1s of TFPT, g-C_3N_4 and TFPT/g-C_3N_4.

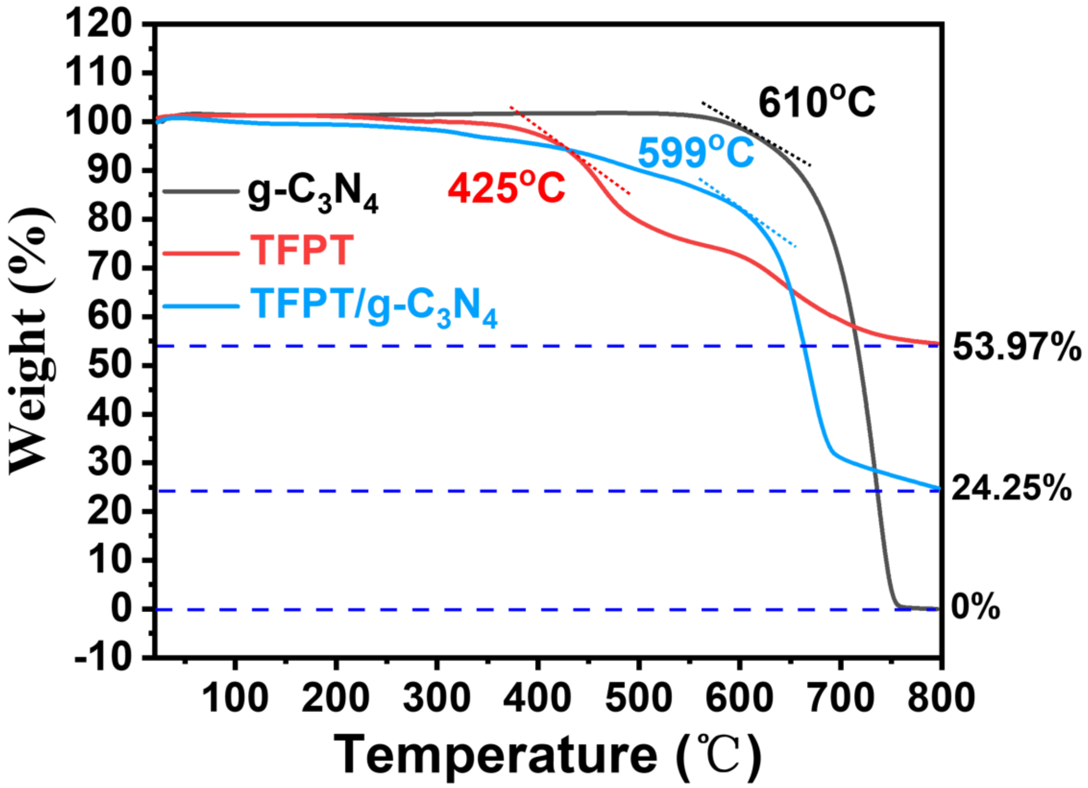

Figure S5. TGA curve of TFPT, g-C_3N_4, and TFPT/g-C_3N_4 obtained under nitrogen atmosphere at a heating rate of 10 °C/min.

The exact proportions of TFPT:g-C_3N_4 from thermogravimetric weight loss:

At 800 °C, the residual rate of g-C_3N_4, TFPT and TFPT/g-C_3N_4 was 0%, 53.97% and 24.25%, respectively. It is assumed that the mass fraction of TFPT in the composite is x, and that of g-C_3N_4 is 1−x. Due to the complete decomposition of g-C_3N_4, the residual rate (24.25%) of the composites was only contributed by TFPT.

$x \times 53.97\% = 24.25\%$; $x = 24.25\%/53.97\% \approx 0.4493$

Accordingly, the mass fraction of the components is determined as follows:

Mass fraction of TFPT: $x \approx 44.93\%$

Mass fraction of g-C_3N_4: $1 - x = 1 - 44.93\% \approx 55.07\%$

Thus, the mass ratio of TFPT:g-C_3N_4 in the TFPT/g-C_3N_4 is calculated as:

$44.93\%:55.07\% \approx 45:55 \approx 9:11$

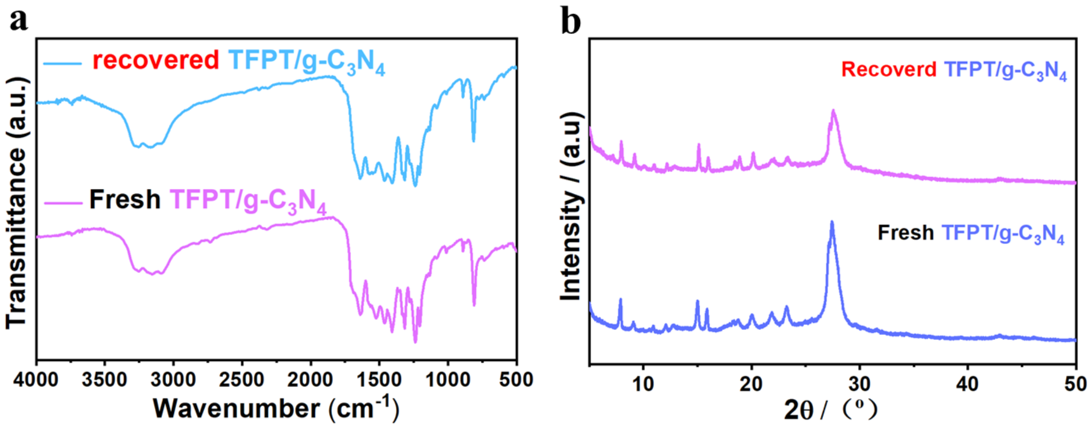

Figure S6. Stability of the catalyst TFPT/g-C_3N_4. (a) IR spectra of "fresh" and "recovered" TFPT/g-C_3N_4; (b) XRD spectra of "fresh" and "recovered" TFPT/g-C_3N_4.

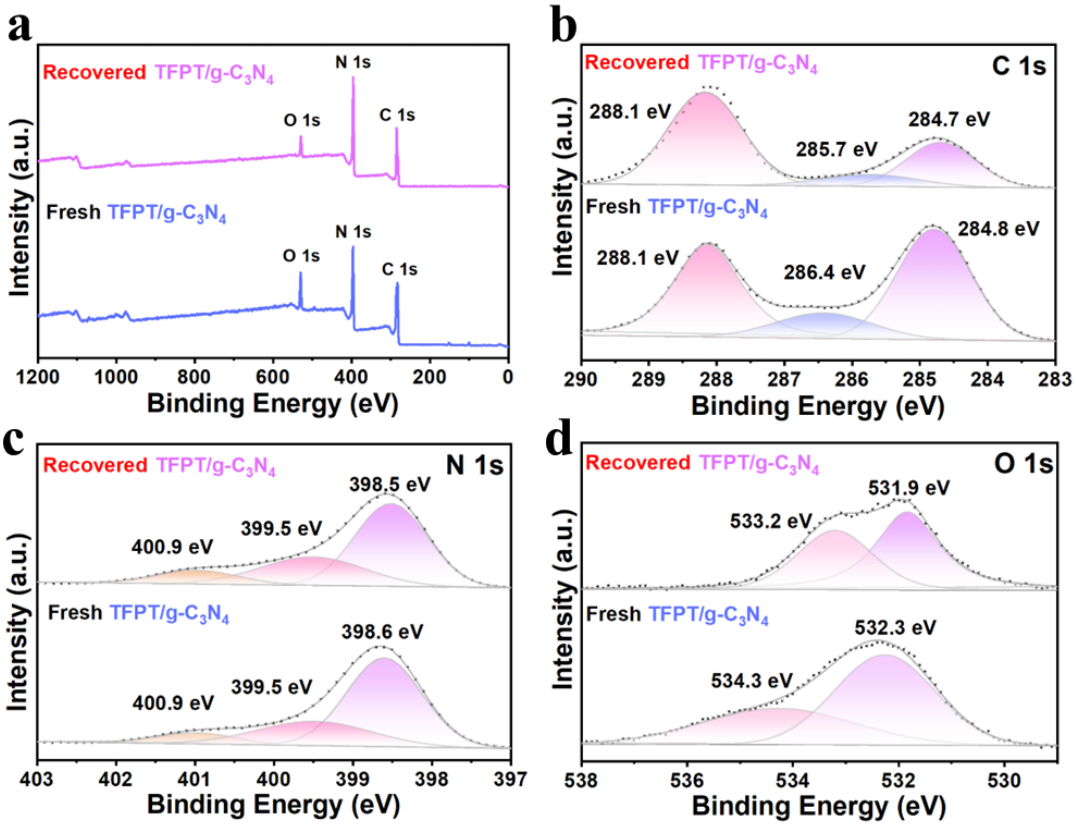

Figure S7. XPS spectra of recovered and fresh TFPT/g-C_3N_4: (A) Survey, (B) C 1s, (C) N 1s, (D) O 1s.

Table S1. Reusability tests using the isolated TFPT/g-C_3N_4 photocatalyst for conversion of PP-ol[a]

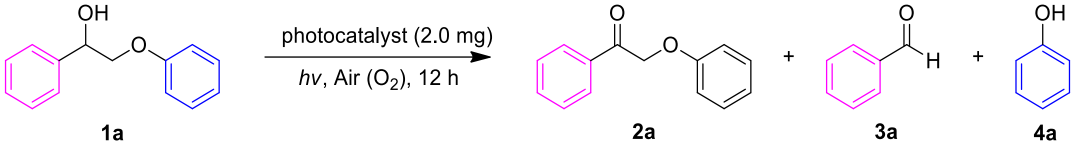

Entry	**1a** conv. (%)	Yield (%)			C_α-C_β Cleavage Sel. (%)
		2a	**3a**	**4a**	
1	94	8	86	33	91.5
2	93	<10	83	29	89.2
3	92	12	80	25	86.9
4	90	15	75	17	83.3

[a] Reaction conditions: 0.2 mmol of PP-ol (**1a**) (1.0 equiv.), photocatalyst (2.0 mg), solvent: MeCN (3 mL), under irradiation with a Xe lamp at room temperature for 12 h.

Table S2. Organic elemental analysis (EA) of TFPT/g-C_3N_4, TFPT and TFPT-150.

Material	Element	Concentration in Solids	Atomic ratio
TFPT/g-C_3N_4	C	42.25%	C/N/H/O = 26.46/27/16.24/1
	N	50.55%	
	O	2.13%	
	H	2.18%	
TFPT	C	70.855	C/N/H/O = 23.99/3/14.83/3.45
	N	10.325	
	O	13.585	
	H	3.675	
TFPT-150	C	71.475	C/N/H/O = 23.82/3/14.29/3.17
	N	10.495	
	O	12.665	
	H	3.60	

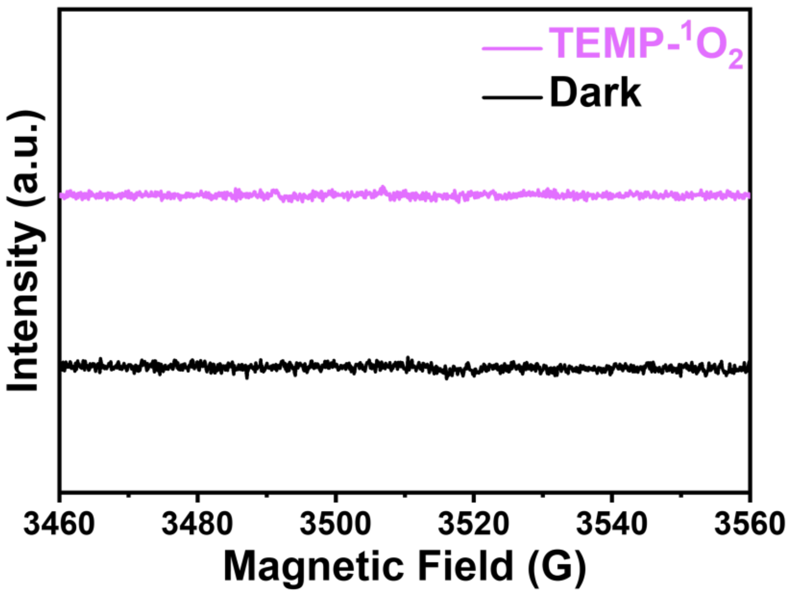

Figure S8. EPR signals of the reaction solution in the dark (black line) and light illumination (pink line) in the presence of TEMP as spin-trapping reagents under experimental conditions. (2,2,6,6-Tetramethyl-4-piperidone hydrochloride = TEMP)

Scheme S1. Mechanistic experiments.

(a) Radical-trapping experiment

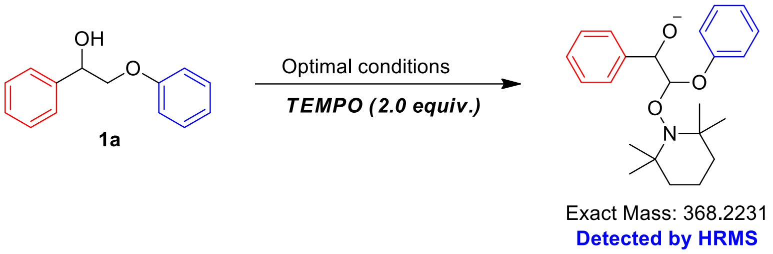

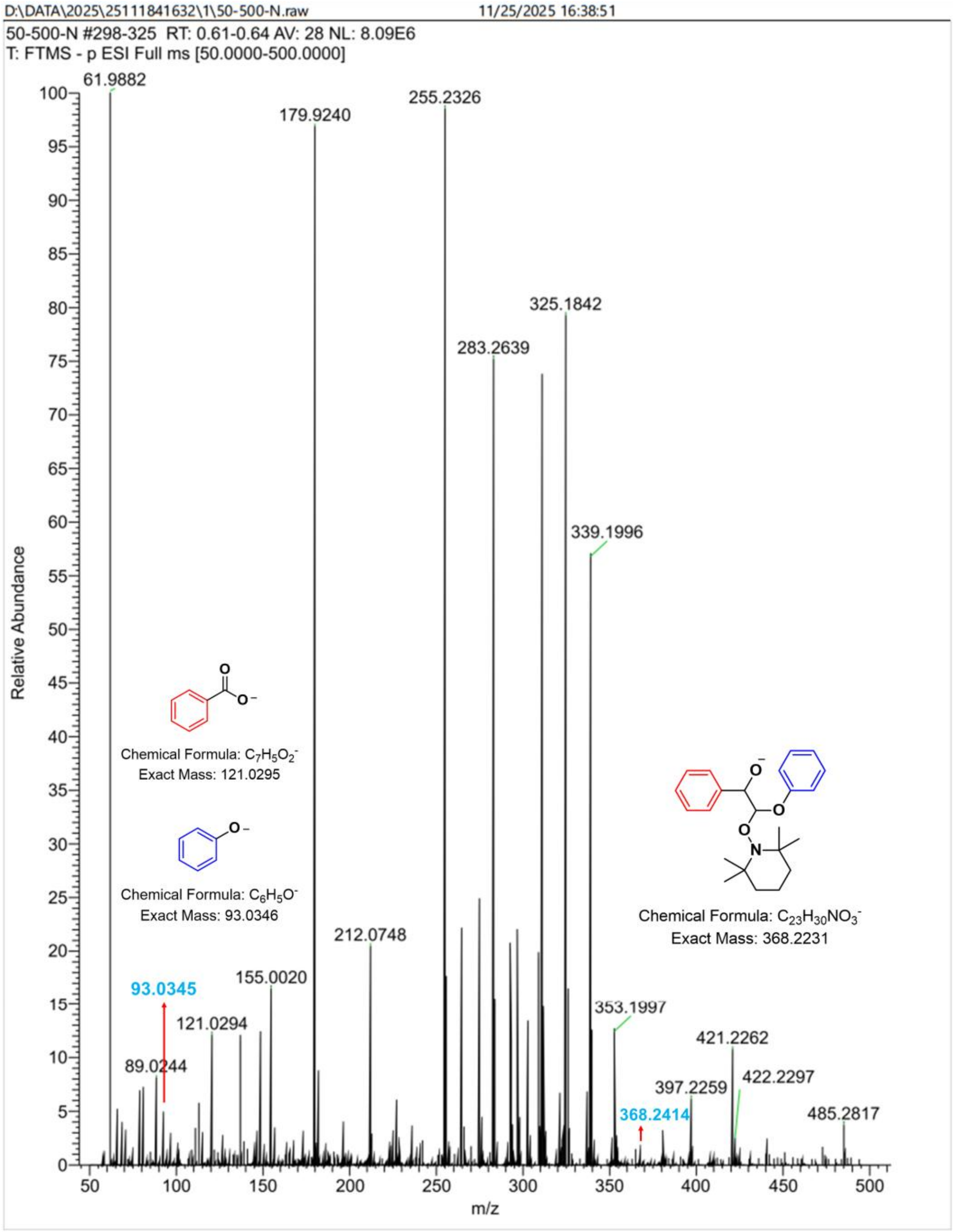

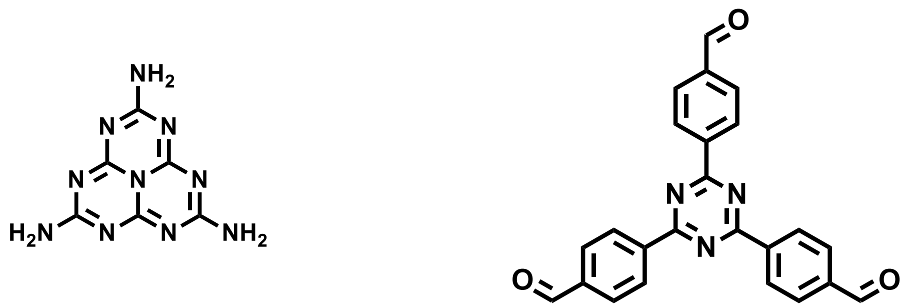

Graphitic carbon nitride (g-C_3N_4) 2,4,6-Tris(4-formylphenyl)-1,3,5-triazine (TFPT)

Scheme S2. The molecular structure of TFPT and the basic structural units of g-C_3N_4.

Table S3. The φ_{red} and corresponding LUMO levels of the TFPT and g-C_3N_4.

Entry	φ_{red} (eV)	E_{LUMO} (eV)
TFPT	-0.690	-3.670
g-C_3N_4	-0.679	-3.681

This electrochemical method was performed following the procedure described in the literature:

1. X.-j. Li, Y.-f. Li, Measurement of electronic energy levels of conjugated polymers and organic molecules, *Acta Polymerica Sinica*, 2022, *53*, 955-1004.
2. H.-J. Lee, E. S. Cho, Selective Photocatalytic C−C Bond Cleavage of Lignin Models and Conversion to High-Value Chemical by Polyoxometalate Under a Mild Water-Based Environment. *ACS Sustainable Chem. Eng.*, **2023**, 11**,** 7624-7632.

Table S4. From each band gap and LUMO value, corresponding HOMO energy levels of TFPT and g-C_3N_4.

Entry	E_{HOMO} (eV)
TFPT	-6.77
g-C_3N_4	-6.631

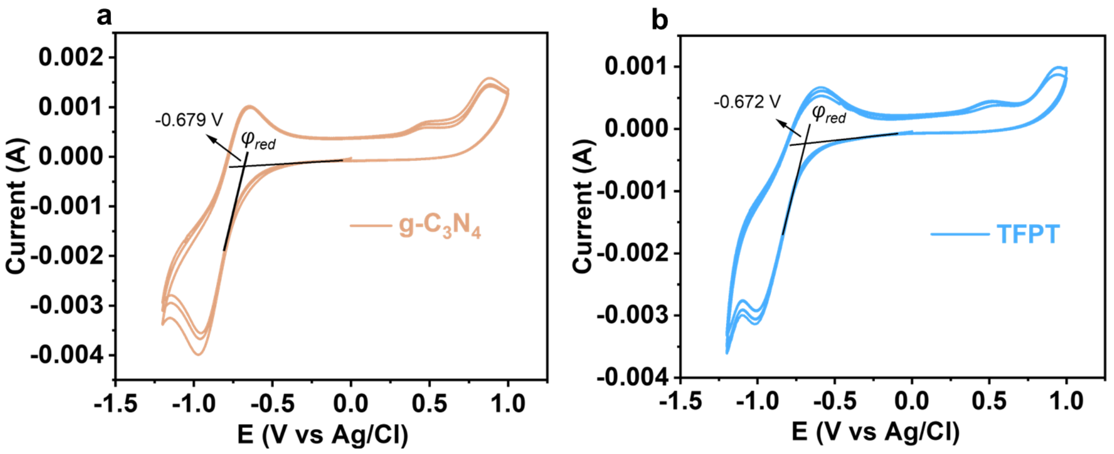

Figure S9. Cyclic voltammograms of the TFPT and g-C_3N_4 measured in 0.1 mol·L^{-1} Bu_4NPF_6 acetonitrile solution.

Table S5. Photocatalytic conversion of PP-ol under different photocatalyst[a]

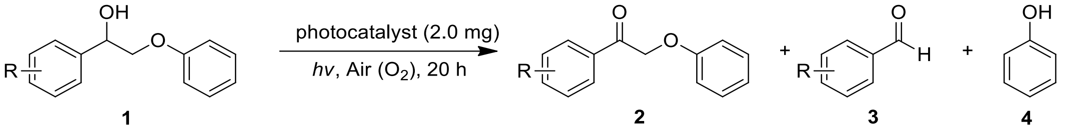

Entry	Substrate	**1** conv. (%)	Yield (%)			Cα-Cβ Cleavage Sel. (%)
			2	**3**	**4**	
1	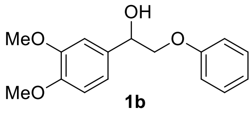 **1b**	31	Trace	21	-	67.7
2	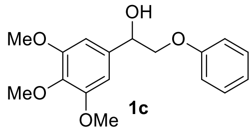 **1c**	26	<5	17	-	65.4

[a]Reaction conditions: 0.1 mmol of (**1**) (1.0 equiv.), photocatalyst (2.0 mg), solvent: MeCN (3 mL), under irradiation with a Xe lamp (300 W) at room temperature for 20 h, "–"means not detected.

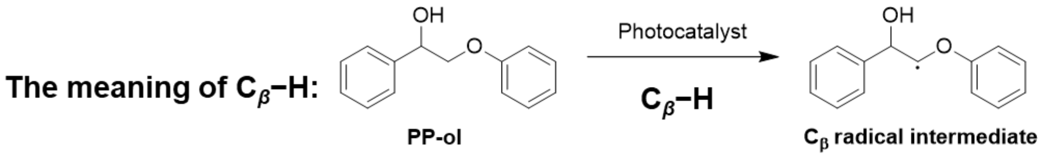

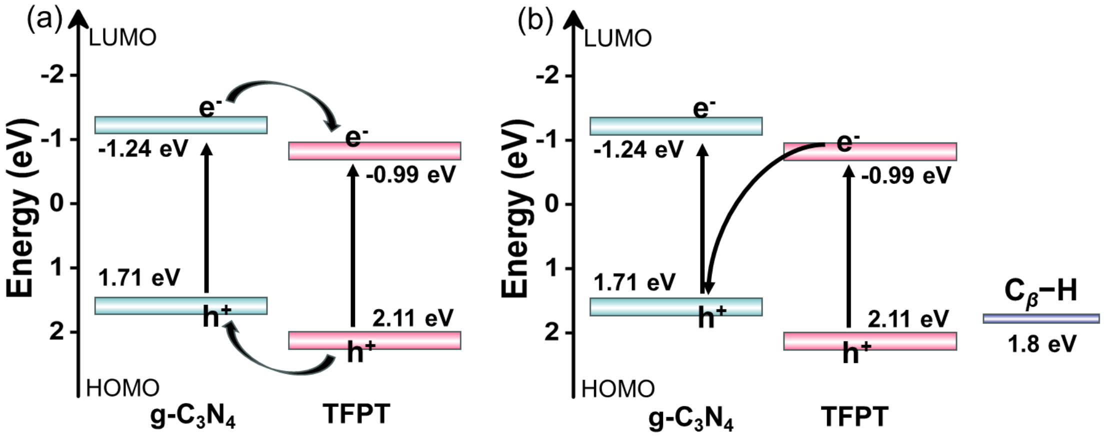

Figure S10. Two models of charge separation proposed for TFPT/g-C_3N_4 under light irradiation: (a) Type-II heterojunction. (b) Direct Z-scheme heterojunction. Energy levels (vs. NHE) are obtained form VB-XPS (**Figure 2f**) and Tauc plot analysis (**Figure S3**).

The type of heterojunction: Based on the experimental results of the HOMO and LUMO energy levels obtained form VB-XPS (Figure 2f) and Tauc plot analysis (Figure S3), two models of charge separation are proposed for TFPT/g-C_3N_4 under light irradiation (Figure S10): Type-II heterojunction and direct Z-scheme heterojunction. Both charge transfer pathways effectively promoted the separation of electron-hole pairs. However, the second pathway (direct Z-scheme) resulted in significantly higher redox capabilities (both oxidability and reducibility). For Type-II heterojunction charge transfer pathway (Figure S10a), the photogenerated hole (h^+) was located at the HOMO of g-C_3N_4 (1.71 eV), which was lower than the potential of oxidation of PP-ol to form C_β radical intermediates (1.80 eV). In contrast, for the direct Z-scheme heterojunction, photogenerated hole (h^+) were located at the HOMO of TFPT (2.11 eV), which was higher than the potential of oxidation of PP-ol to form C_β radical intermediates (1.80 eV). That is to say, for Z-scheme charge transfer pathway, the photogenerated hole (h^+) could oxidize the PP-ol to form C_β radical intermediates, and the C_β radical intermediates could further react with superoxide anion radical ($^\bullet O_2^-$) to complete the catalytic cycle. Conversely, for the Type-II heterojunction charge transfer pathway, photogenerated hole (h^+) couldn't oxidize the PP-ol to form C_β radical intermediates. Using the high-resolution mass spectrometry (HRMS, Scheme S1), the C_β radical intermediates were detected as adducts with TEMPO. The results proved that the charge transfer pathway in the TFPT/g-C_3N_4 was a direct Z-scheme heterojunction.

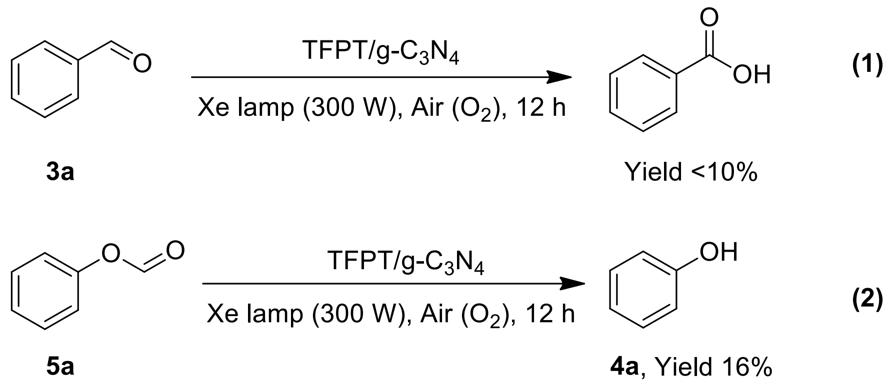

Scheme S3. Control experiments.

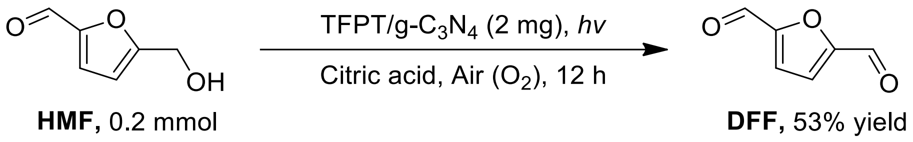

Scheme S4. The photocatalytic performance of HMF over TFPT/g-C_3N_4.

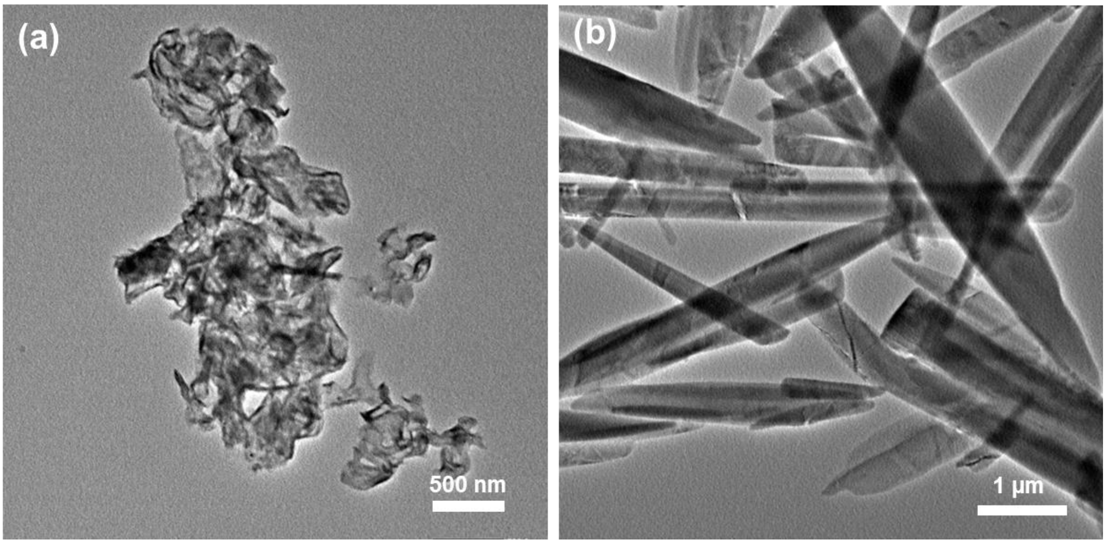

Figure S11. TEM images of (a) g-C_3N_4 and (b) TFPT.

Table S6. Photocatalytic conversion of PP-ol under different light sources[a]

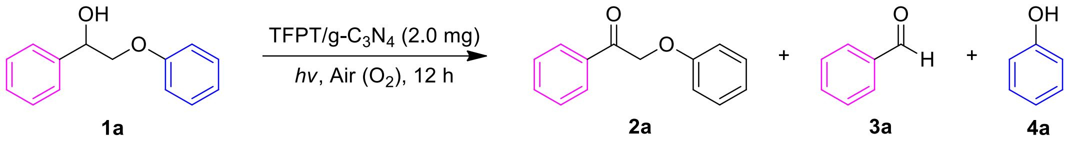

Entry	**1a** conv. (%)	*hv* (nm)	Yield (%)			C_α-C_β Cleavage Sel. (%)
			2a	**3a**	**4a**	
1	49	400-415	trace	47%	trace	95.9
2	54	435-445	33	12	trace	22.2
3	no	450-455	-	-	-	-
4	<5	460-475	-	<5	-	-
5	no	475-485	-	-	-	-

[a] Reaction conditions: 0.2 mmol of PP-ol (**1a**) (1.0 equiv.), photocatalyst (2.0 mg), solvent: MeCN (3 mL), under irradiation with a Xe lamp at room temperature for 12 h.

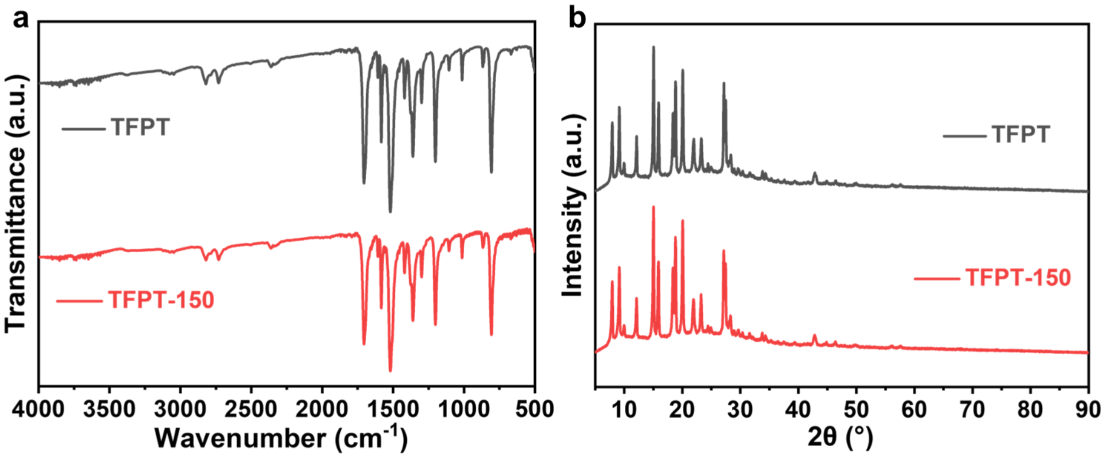

Figure S12. Stability of the TFPT catalyst after heating at 150°C for 12 h during the preparation process. (a) FTIR spectra and (b) XRD spectra of TFPT and TFPT-150.

^{1}H NMR spectroscopic data of DFF, **3a, 3b** and **3c.**

Furan-2,5-dicarbaldehyde (DFF), ^{1}H NMR (500 MHz, $CDCl_3$) δ 9.89 (s, 2H), 7.36 (s, 2H).

Benzaldehyde (**3a**).^{1}H NMR (500 MHz, $CDCl_3$) δ 10.02 (s, 1H), 7.94–7.85 (m, 2H), 7.64 (t, J = 7.4 Hz, 1H), 7.54 (t, J = 7.6 Hz, 2H).

3,4-dimethoxybenzaldehyde (**3b**). ^{1}H NMR (400 MHz, $CDCl_3$) δ 9.86 (s, 1H), 7.47 (dd, J = 8.2, 1.9 Hz, 1H), 7.42 (d, J = 1.9 Hz, 1H), 6.99 (d, J = 8.2 Hz, 1H), 3.97 (s, 3H), 3.95 (s, 3H).

3,4,5-trimethoxybenzaldehyde (**3c**). ^{1}H NMR (400 MHz, $CDCl_3$) δ 9.87 (s, 1H), 7.21 (d, J = 59.9 Hz, 2H), 3.95 (s, 3H), 3.94 (s, 6H).

(1) C. Ayed, W. Huang, G. Kizilsavas, K. Landfester, K. a. I. Zhang, *ChemPhotoChem*, **2020**, 4, 571-576.

(2) S. Li, U. K. Wijethunga, C. Chu, S. Kim, W. Zheng, B. D. Sherman, C. G. Yoo, S. Lee, G. Leem, *ACS Catal.*, **2025**, 15, 4460-4467.

(3) K. Lee, R. E. Maleczka, *Org. Lett.*, **2006**, 8, 1887-1888.

^{1}H NMR spectra of DFF**.**

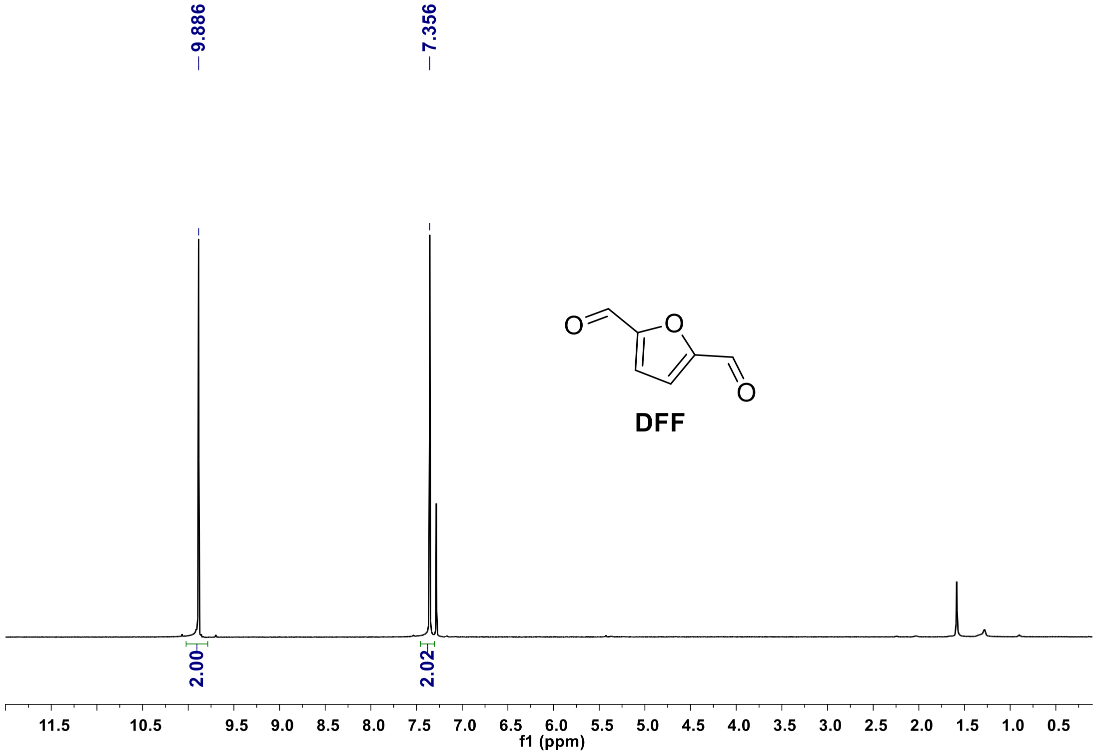

^{1}H NMR spectra of **3a.**

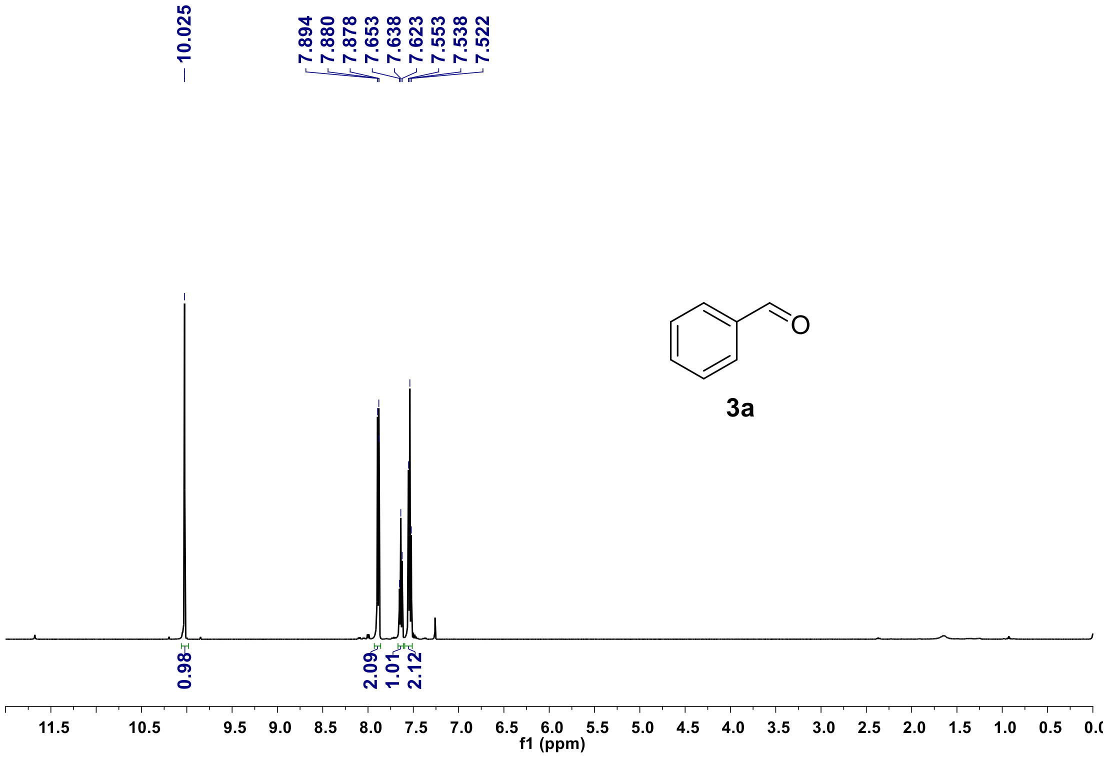

^{1}H NMR spectra of **3b.**

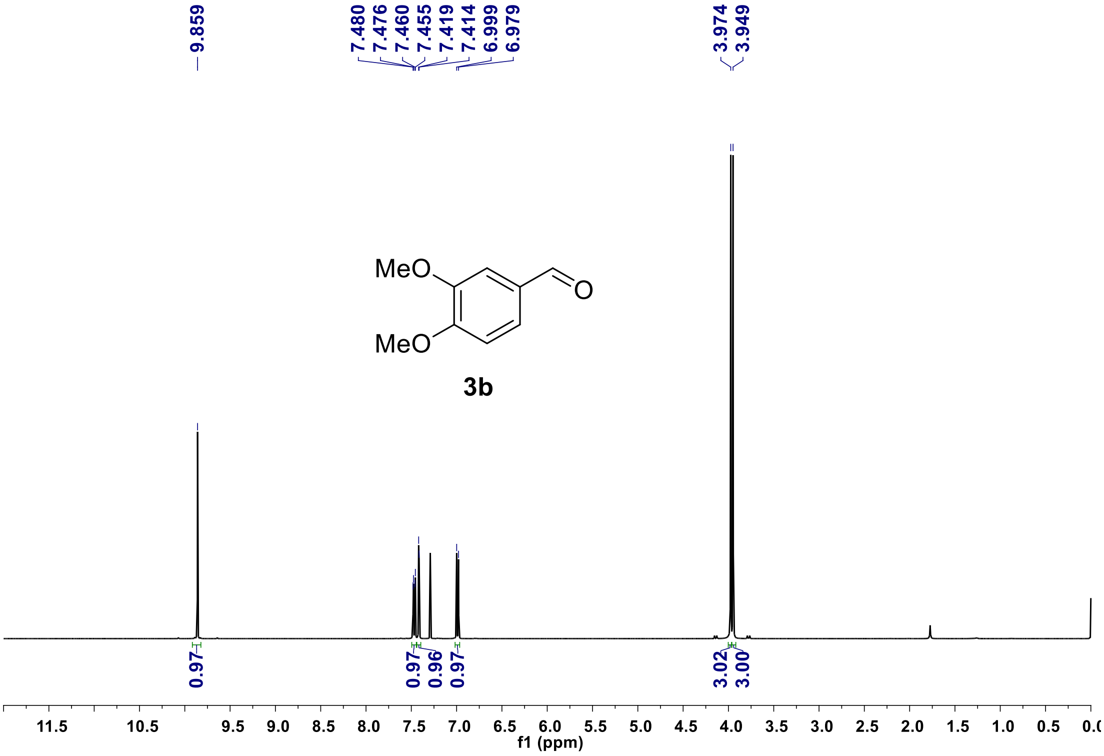

^{1}H NMR spectra of **3c.**